where ϵ^α is the internal energy of the α^{th} constituent, ϵ_S^α is the energy supply to the α^{th} constituent, $\mathbf{q}^\alpha$ is the heat conduction associated with α^{th} constituent and r^α is the radiant heat supply to the α^{th} constituent.

7 Second Law of Thermodynamics

Even when attention is focused on enforcing the second law of thermodynamics in its local form, there are two different points of view in mixture theory. The first requires that the second law hold for each constituent while the other requires that it holds for the mixture as a whole. Even after one makes a decision with regard to how we decide to enforce the second law, it is important to recognize that there is not yet an agreement as to what form the second law should take, whether one should interpret it as the Planck inequality, Kelvin–Planck inequality, the Clausius inequality, the Clausius–Duhem inequality (see Coleman and Noll [6]), the approach adopted by Caratheodory, or the more recent choice wherein an constitutive assumption is made for the structure of the rate of entropy production which is required to be non-negative (see the approaches of Ziegler [42–44], and those of Rajagopal and Srinivasa [30–32]; the approaches are quite different though at first glance can be mistaken to be similar, see the extended discussion in Rajagopal and Srinivasa [31] for the differences between the two approaches), or a whole host of other approaches. We shall not get into a discussion of these issues here but use the simple approach that the second law is to be satisfied for the mixture as a whole and not the individual constituents, and furthermore enforce the second law in the form

$$\frac{\partial}{\partial t}\Big(\sum_{\alpha=1}^{N}\rho^\alpha\eta^\alpha\Big)+\operatorname{div}\Big(\sum_{\alpha=1}^{N}\rho^\alpha\eta^\alpha\mathbf{v}\Big)+\operatorname{div}\Big(\sum_{\alpha=1}^{N}\frac{\mathbf{q}^\alpha+\rho^\alpha\eta^\alpha\theta^\alpha\mathbf{v}}{\theta^\alpha}\Big)-\sum_{\alpha=1}^{N}\frac{\rho^\alpha r^\alpha}{\theta^\alpha}\geq 0, \tag{26}$$

where θ^α, $\mathbf{q}^\alpha$, η^α, and r^α are the absolute temperature, heat flux vector, specific entropy, and the specific radiant heating associated with the α^{th} constituent.

A detailed discussion of the rationale for using the second law for the mixture as a whole, and the derivation and explanation of the terms that appear in the above equation can be found in Rajagopal and Tao [33].

8 Volume Additivity Constraint

In addition to the above balance laws and the entropy production inequality, just as in the case of a single constituent continuum we might have to enforce constraints such as incompressibility or inextensibility. A constraint that is often used in the

theory of mixtures is that of the additivity of the volumes of the constituents (see Mills [22]). This is different from the requirement that each of the constituents is individually incompressible, it is a much weaker assumption and gives rise to just one Lagrange multiplier. Also, from a physical standpoint, allowing each constituent to be incompressible presents a fundamental problem as each constituent also occupies, in a homogenized sense, the whole space occupied by the mixture. This would mean that the mapping that takes the reference configuration for the pure constituent to that of the mixture cannot be iso-choric, or put physically one cannot spread a pure incompressible constituent from its reference state to the current state of the mixture which is the sum of the volume of all the constituents. As we shall just consider two constituents later, namely water and ice, we shall document the volume additivity constraint in the case of these two constituents:

$$\frac{\rho^I}{\rho_R^I}(1-\beta)+\frac{\rho^W}{\rho_R^W}=1, \tag{27}$$

where β is the porosity of ice, the superscripts I and W denote ice and water, and the subscript R denotes that the quantity in question refers to its value in the pure constituent configuration. The above can be described in the equivalent Eulerian form:

$$\frac{\rho^I}{\rho_R^I}\operatorname{div}\mathbf{v}^I+\frac{1}{1-\beta}\frac{\rho^W}{\rho_R^W}\operatorname{div}\mathbf{v}^W+\nabla\left(\frac{\rho^I}{\rho_R^I}\right)\cdot(\mathbf{v}^I-\mathbf{v}^W)=0. \tag{28}$$

9 Issues Concerning Boundary Conditions for Mixtures

In order to solve the appropriate initial-boundary value problem, it is necessary to be able to prescribe appropriate boundary conditions. This is no easy task due to the assumption of co-occupancy. While one knows the total traction on the mixture, one does not know how this splits into partial tractions supported by the individual constituents on the parts of the domain where traction is specified. Similarly, while we might know the displacement or velocity of the mixture on parts of the boundary but not the individual displacements associated with the constituents (see Rajagopal and Tao [33] for detailed discussion of this issue). When one is dealing with a solid that swells significantly when infused with a fluid, like a sponge absorbing water or polymers and biological matter that undergo significant dimensional changes due to absorbing water, one can appeal to a variety of boundary conditions: (1) A boundary condition that stems from assuming that the boundary of the swollen solid that is in contact with the fluid is saturated (see Rajagopal et al. [34]); (2) Splitting the traction based on purely mechanical considerations (see Rajagopal and Tao [33]); (3) The assumption that the chemical potential is continuous across the boundary between the swollen solid and the fluid. When dealing with a mixture of ice and

water, splitting the traction based the mass or volume fraction of the two constituents may be the best option.

10 Simplified Equations

We shall assume that there are only two constituents (the two phases: water and ice) in the mixture and there is the possibility of conversion between the phases. Furthermore, as a first step at studying the problem, we shall ignore the energy equation and study just the system of equations comprising those of mass and momentum balance for both the constituents, and even this simplified system reduces to eight coupled partial differential equations. In a future study, we shall consider the full thermodynamic problem that includes the balance of energy for the two phases as well as the second law of thermodynamics, which will add two more partial differential equations and a differential inequality.

In this case, the balance of mass reduces to:

$$\frac{\partial \rho^W}{\partial t} + \operatorname{div}(\rho^W \mathbf{v}^W) = m, \tag{29}$$

and

$$\frac{\partial \rho^I}{\partial t} + \operatorname{div}(\rho^I \mathbf{v}^I) = -m, \tag{30}$$

where m denotes the conversion of ice into water. Since we consider only two constituents, the production of one of the constituents is at the expense of the reduction of the other and hence $m^W = -m^I = m$. Next, we will assume that the partial stress tensors associated with both the phases is symmetric. Then, the balances of linear momenta reduce to:

$$\operatorname{div}(\mathbf{T}^W) + \rho^W \mathbf{b}^W + \mathbf{m}^W + m\mathbf{v}^W = \frac{\partial}{\partial t}(\rho^W \mathbf{v}^W) + \operatorname{div}(\rho^W \mathbf{v}^W \otimes \mathbf{v}^W), \tag{31}$$

and

$$\operatorname{div}(\mathbf{T}^I) + \rho^I \mathbf{b}^I + \mathbf{m}^I - m\mathbf{v}^I = \frac{\partial}{\partial t}(\rho^I \mathbf{v}^I) + \operatorname{div}(\rho^I \mathbf{v}^I \otimes \mathbf{v}^I). \tag{32}$$

We shall assume that

$$\mathbf{m}^W + \mathbf{m}^I + m(\mathbf{v}^W - \mathbf{v}^I) = 0. \tag{33}$$

We shall also assume that the body force acting on both the constituents is gravity, which we will denote by **g**. Thus, the above equations reduce to

$$\operatorname{div}(\mathbf{T}^W) + \rho^W \mathbf{g} + \mathbf{m}^W + m\mathbf{v}^W = \frac{\partial}{\partial t}(\rho^W \mathbf{v}^W) + \operatorname{div}(\rho^W \mathbf{v}^W \otimes \mathbf{v}^W), \tag{34}$$

$$\operatorname{div}(\mathbf{T}^I) + \rho^I \mathbf{g} + \mathbf{m}^I - m\mathbf{v}^I = \frac{\partial}{\partial t}(\rho^I \mathbf{v}^I) + \operatorname{div}(\rho^I \mathbf{v}^I \otimes \mathbf{v}^I), \tag{35}$$

where **g** is the acceleration due to gravity. Since we have assumed that the stress tensors are symmetric, it follows from the balance of angular momentum that there can be no angular momentum supply to either of the constituents. The governing equations for the specific model under consideration are obtained by substituting the appropriate constitutive expressions for the production of water m, the interaction force **m** (discussed in Sect. 12) and the constitutive assumptions for the partial stresses for water and ice, $\mathbf{T}^w$ and $\mathbf{T}^I$, respectively.

11 Constitutive Relations: Model for Water and Ice

We shall model water as a Navier–Stokes fluid whose viscosity depends on temperature. Thus, we shall model the Cauchy stress in water through

$$\mathbf{T}^W = -p_{\text{thm}}(\rho^W, \theta)\mathbf{I} + \lambda^W(\rho^W, \theta)\operatorname{tr}(\mathbf{A}_1^W)\mathbf{I} + \mu^W(\rho^W, \theta)\mathbf{A}_1^W, \tag{36}$$

where **I** is the unit tensor, p_{thm} denotes the thermodynamic pressure of water that is assumed to be compressible, albeit slightly, in the temperature range of interest, ρ^W is the density of water, λ^W and μ^W are the bulk and shear viscosities of water, θ is the absolute temperature, and

$$\mathbf{A}_1^W = \frac{\partial \mathbf{v}^W}{\partial \mathbf{x}} + \left(\frac{\partial \mathbf{v}^W}{\partial \mathbf{x}}\right)^{\mathrm{T}} = 2\mathbf{D}^{\mathbf{W}}. \tag{37}$$

The constitutive relation for ice depends on the time scale of interest. If one is concerned with long term response of ice sheets, they behave as though they are fluid-like. The popular model for ice is that which was proposed by Glen [10] to characterize the response of ice, as a power-law fluid model. But this model is incapable of describing normal stress differences in simple shear flow that has been observed in ice (see Kjartson et al. [18], Man and Sun [19]). A simple model that allows for the shear thinning as well as the normal stress differences observed in ice is the following:

$$\mathbf{T}^I = -p\mathbf{I} + \mu^I(\mathbf{A}_1^I, \theta)\mathbf{A}_1^I + \alpha_1 \mathbf{A}_2^I + \alpha_2 \mathbf{A}_1^I, \tag{38}$$

where μ^I is the viscosity of ice, and α_1 and α_2 are the normal stress coefficients (which for the sake of simplicity we shall assume to be constant), and

$$\mathbf{A}_2^I = \frac{d\mathbf{A}_1^I}{dt} + \mathbf{A}_1^I \mathbf{L}^I + (\mathbf{L}^I)^{\mathrm{T}} \mathbf{A}_1^I, \tag{39}$$

where $\frac{d}{dt}$ is the material time derivative (see (9)), and $\mathbf{A}_1^I$ and $\mathbf{A}_2^I$ are the first two Rivlin–Ericksen tensors (see Rivlin and Ericksen [35]). We shall assume a power-law form for the generalized viscosity, namely

$$\mu^I(\mathbf{A}_1^I, \theta) = \hat{\mu}(\theta) \left[1 + \lambda(\mathrm{tr}(\mathbf{A}_1^I)^2)\right]^n, \tag{40}$$

where n is the power-law exponent and λ is a constant.

A critical and detailed discussion of the fluids of the differential type, the class to which the above model belongs, can be found in the review article by Dunn and Rajagopal [8]. The above model does not allow for ice to exhibit stress-relaxation. Stress-relaxation does not seem to be an important characteristic of ice and hence we shall use the simple model (38). If one requires a model that can also exhibit stress relaxation, then one could use a generalized rate type model that can describe shear thinning, stress-relaxation, nonlinear creep and normal stress differences in simple shear flow, namely a modified Maxwell model:

$$\mathbf{T}^I = -p^I \mathbf{I} + \mathbf{S}^I, \tag{41}$$

$$\mathbf{S}^I + \lambda \overset{\triangledown}{\mathbf{S}}{}^I = \eta(\mathbf{A}_1^I)\mathbf{A}_1^I, \tag{42}$$

where $-p^I\mathbf{I}$ is the indeterminate part of the stress due to the constraint of incompressibility, λ is the relaxation time, $\eta(\mathbf{A}_1^I)$ is the generalized viscosity and the upper convected Oldroyd derivative $\overset{\triangledown}{\mathbf{B}}$ is defined through

$$\overset{\triangledown}{\mathbf{B}} = \frac{d\mathbf{B}}{dt} - \mathbf{L}\mathbf{B} - \mathbf{B}\mathbf{L}^{\mathrm{T}}, \tag{43}$$

for any tensor $\mathbf{B}$.

12 Constitutive Assumption for the Interaction Terms

A key aspect of the constitutive theory for mixtures is the specification of interaction forces $\mathbf{m}^\alpha$ which can be used to incorporate the effect of drag due to the difference in velocity, the virtual mass effect, Magnus effect due to the relative spin, the effect of relative history of motion, the differences in the densities, etc., all of them between

the various constituents, (see Johnson et al. [16] for a detailed discussion of the interaction mechanisms). In this work, in addition to taking into account the mass that is generated due to phase change, we have to take into account interaction terms that come into play, both in the balance of linear momentum and the balance of energy due to phase change. With regard to the interaction terms that come into play in the balance of linear momentum, as the flows involved are reasonably slow, we can ignore effects such as the virtual mass effect that are a consequence of the difference in the acceleration of the constituents. We shall also ignore the effects of relative spin, relative histories, etc. The only interaction terms that we shall take into account are due to the relative velocities, namely the Drag, and the interaction term that is a consequence of the phase change. Thus, we shall assume that

$$\mathbf{m}^W = \alpha(\theta)(\mathbf{v}^W - \mathbf{v}^I) + \lambda^{IW}, \tag{44}$$

where α is the Drag coefficient and λ^{IW} denotes the contribution to the momentum of water due to phase change. Similarly

$$\mathbf{m}^I = \alpha(\theta)(\mathbf{v}^I - \mathbf{v}^W) + \lambda^{WI}, \tag{45}$$

and

$$\lambda^{WI} \neq -\lambda^{IW}. \tag{46}$$

Specific constitutive choices have to be made for λ^{IW}, λ^{WI} and m^α and these should be based on observations and carefully carried out experiments. We can start by assuming simple forms such as those used by Morland et al. [25]. In a comprehensive study that also includes the energy equation and the second law of thermodynamics, we would have to specify constitutive relations for the internal energy of each of the constituents, the energy supply ϵ^α, heat flux vector associated with each constituent $\mathbf{q}^\alpha$, and the radiant energy supply r^α.

13 Governing Equations

Based on the above balance laws, the second law of thermodynamics, the volume additivity constraint and constitutive relations, we have to obtain the governing partial differential equations, and the inequality that stems from the second law. Further simplifications can then be made that apply to the problem on hand. For instance, as we shall be interested in the sea ice flow in the Arctic, we expect the flow to be slow and thus we can neglect the inertial term in the balance of linear momentum for the constituents. Also, as mentioned earlier, we can associate a single temperature with both the constituents, water and ice. In this short paper we are merely interested in documenting the basic balance laws and the constitutive

relations that will be used to develop the governing equations. In future work we will present the mathematical analysis of specific simplified models.

Acknowledgement KRR thanks the Office of Naval Research for support of this work.

References

1. Atkin, R.J., Craine, R.E.: Continuum theories of mixtures: basic theory and historical development. Q. J. Mech. Appl. Math. **29**, 209–244 (1976)
2. Atkin, R.J., Craine, R.E.: Theories of mixtures: applications. J. Inst. Math. Appl. **17**, 153–207 (1976)
3. Bedford, A., Drumheller, D.S.: Theory of immiscible and structured mixtures. Int. J. Eng. Sci. **21**, 863–960 (1983)
4. Bowen, R.: In: Eringen, A.C. (ed.) Theory of Mixtures in Continuum Physics III. Academic, New York (1976)
5. Bushuk, M., Giannakis, D., Majda, A.J.: Arctic sea ice reemergence: the role of large-scale oceanic and atmospheric variability. J. Climate **28**, 5477–5509 (2015)
6. Coleman, B.D., Noll, W.: An approximation theorem for functionals, with applications in continuum mechanics. Arch. Ration. Mech. Anal. **6**, 355–370 (1960)
7. Darcy, W.: Les Fontaines Publiques de La Ville de Dijon. Dalmont, Paris (1856)
8. Dunn, J.E., Rajagopal, K.R.: Fluids of differential type: critical review and thermodynamic analysis. Int. J. Eng. Sci. **33**, 689–729 (1995)
9. Fick, A.: Ueber diffusion. Ann. Phys. **94**, 59–86 (1855)
10. Glen, J.W.: The flow law of ice: a discussion of assumptions made in glacier theory, their experimental foundations and consequences, in the Physics of the Movement of Ice. Int. J. Assoc. Sci. Hydrol. Publ. **47**, 171–183 (1958)
11. Gray, J.M.N.T., Morland, L.W.: A two-dimensional model for the dynamics of sea ice. Philos. Trans. Phys. Sci. Eng. **347**(1682), 219–290 (1994)
12. Green, A.E., Naghdi, P.M.: On basic equations for mixtures. Q. J. Mech. Appl. Math. **XXII**, 427–438 (1969)
13. Hunke, E.C., Dukowicz, J.K.: An elastic-viscous-plastic model for sea ice dynamics. J. Phys. Oceanogr. **27**, 1849–1867 (1997)
14. Hutter, K.: Theoretical Glaciology: Material Science of Ice and the Mechanics of Glaciers and Ice Sheets. D. Reidell, Norwell (1983)
15. Hutter, K., Blatter, H., Funk, M.: A model computation of moisture content in polythermal ice sheets. J. Geophys. Res. **93**, 12205–12214 (1988)
16. Johnson, G., Massoudi, M., Rajagopal, K.R.: A review of interaction mechanisms in fluid-solid flows, DOE/PETCLTR90/9, DE 91 0000941, Pittsburgh, PA (1991)
17. Kelly, R.J., Morland, L., Morris, E.M.: A three phase mixture model for melting snow. In: Modelling Snowmelt-induced Processes, vol. 155, pp. 17–26. IAHS Publications, Wallingford (1986)
18. Kjartanson, B.H., Shields, D.H., Domaschuk, L., Man, C.S.: The creep of ice measured with the pressuremeter. Can. Geotech. J. **25**, 250–261 (1988)
19. Man, C.S., Sun, Q.X.: On the significance of normal stress effects in the flow of glaciers. J. Glaciol. **33**, 268–273 (1987)
20. Marshall, S.J., Clarke, G.K.C.: Sensitivity analyses of coupled ice sheet/ice stream dynamics on the EISMINT experimental ice block. Ann. Geol. **23**, 336–347 (1996)
21. Marshall, S.J., Clarke, G.K.C.: A continuum mixture model for ice stream thermomechanics in the Laurentide ice sheet. J. Geophys. Res. **102**, 20599–20613 (1997)
22. Mills, N.: Incompressible mixtures of newtonian fluids. Int. J. Eng. Sci. **4**, 97–112 (1966)

23. Morland, L.: A simple constitutive theory for fluid saturated porous solid. J. Geophys. Res. **77**, 890–900 (1972)
24. Morland, L.: A theory of slow fluid flow through a thermoelastic porous solid. Geophys. J. Res. Astron. Soc. **55**, 393–410 (1978)
25. Morland, L., Kelly, R.J., Morris, E.M.: A mixture theory for phase-changing snowpack. Cold Reg. Sci. Technol. **17**, 271–285 (1990)
26. Morris, E.M.: Modelling the flow of mass and energy within a snowpack for hydrological forecasting. Ann. Glaciol. **4**, 198–203 (1986)
27. Perovich, D.K., Richter-Menge, J.R.: Loss of sea ice in the Arctic. Annu. Rev. Marine Sci. **1**, 417–441 (2009)
28. Prasad, S.C., Rajagopal, K.R.: On the diffusion of fluids through solids undergoing large deformations. Math. Mech. Solids **11**, 91–105 (2006)
29. Rajagopal, K.R.: On an hierarchy of approximate models for flows of incompressible fluids through porous solids. Math. Methods Models Appl. Sci. **17**, 215–252 (2007)
30. Rajagopal, K.R., Srinivasa, A.R.: A thermodynamic framework for rate type fluid models. J. Non-Newtonian Fluid Mech. **88**, 207–227 (2000)
31. Rajagopal, K.R., Srinivasa, A.R.: Thermomechanics of materials that have multiple natural configurations: Part 1 Viscoelasticity and classical plasticity. Z. Angew. Math. Phys. **55**, 861–893 (2004)
32. Rajagopal, K.R., Srinivasa, A.R.: On the thermodynamics of fluids defined by implicit constitutive relations. Z. Angew. Math. Phys. **59**, 715–729 (2008)
33. Rajagopal, K.R., Tao, L.: Mechanics of Mixtures. World Scientific, Singapore (1995)
34. Rajagopal, K.R., Wineman, A.S., Gandhi, M.V.: On boundary conditions for a certain class of problems in mixture theory. Int. J. Eng. Sci. **24**, 1453–1463 (1986)
35. Rivlin, R.S., Ericksen, J.L.: Stress deformation relations for isotropic materials. J. Ration. Mech. Anal. **4**, 323–425 (1955)
36. Samohyl, I.: Thermodynamics of Irreversible processes in Fluid Mixtures. Teubner, Leipzig (1987)
37. Shi, J.J., Rajagopal, K.R., Wineman, A.S.: Application of the theory of interacting continua to the diffusion of a fluid through a non-linear elastic media. Int. J. Eng. Sci. **19**, 871–889 (1981)
38. Truesdell, C.: Sulla basi della termomeccanica, Accademia Nazionale dei Lincei, Rendiconti della Classe di Scienze Fisiche, Mathematiche e Naturali (8) **22**, 33–88 (1957)
39. Truesdell, C.: Sulla basi della termomeccanica, Accademia Nazionale dei Lincei, Rendiconti della Classe di Scienze Fisiche, Mathematiche e Naturali (8) **22**, 158–166 (1957)
40. Truesdell, C.: Rational Thermodynamics. Springer, New York (1984)
41. Truesdell, C., Toupin, R.: The classical field theories. In: Flugge, W. (ed.) Handbuch der Physik, vol. III. Springer, New York (1960)
42. Ziegler, H.: Some extremum principles in irreversible thermodynamics. In: Sneddon, I.N., Hill, R. (eds.) Progress in Solid Mechanics, vol. 4. North Holland Publishing Company, New York (1963)
43. Ziegler, H.: An Introduction to Thermodynamics. North-Holland Series in Applied Mathematics and Mechanics, 2nd edn. North-Holland, Amsterdam (1983)
44. Ziegler, H., Wehrli, C.: The derivation of constitutive equations from the free energy and the dissipation function. In: Wu, T.Y., Hutchinson, J.W. (eds.) Advances in Applied Mechanics, vol. 25, pp. 183–238. Academic Press, New York (1987)

Modelling Sea Ice and Melt Ponds Evolution: Sensitivity to Microscale Heat Transfer Mechanisms

Andrea Scagliarini, Enrico Calzavarini, Daniela Mansutti, and Federico Toschi

Abstract We present a mathematical model describing the evolution of sea ice and meltwater during summer. The system is described by two coupled partial differential equations for the ice thickness h and pond depth w fields. We test the sensitivity of the model to variations of parameters controlling fluid-dynamic processes at the pond level, namely the variation of turbulent heat flux with pond depth and the lateral melting of ice enclosing a pond. We observe that different heat flux scalings determine different rates of total surface ablations, while the system is relatively robust in terms of probability distributions of pond surface areas. Finally, we study pond morphology in terms of fractal dimensions, showing that the role of lateral melting is minor, whereas there is evidence of an impact from the initial sea ice topography.

Keywords Glaciology · Sea ice · Turbulent heat transfer · Mathematical Modelling

A. Scagliarini (✉) · D. Mansutti
Istituto per le Applicazioni del Calcolo 'M. Picone', CNR, Rome, Italy
e-mail: andrea.scagliarini@cnr.it; d.mansutti@iac.cnr.it

E. Calzavarini
Université de Lille, Unité de Mécanique de Lille, UML EA 7512, Lille, France
e-mail: enrico.calzavarini@polytech-lille.fr

F. Toschi
Eindhoven University of Technology, Eindhoven, The Netherlands

Istituto per le Applicazioni del Calcolo 'M. Picone', CNR, Rome, Italy
e-mail: f.toschi@tue.nl

P. Cannarsa et al. (eds.), *Mathematical Approach to Climate Change and Its Impacts*, Springer INdAM Series 38,
https://doi.org/10.1007/978-3-030-38669-6_6

1 Introduction

The Arctic Ocean is characterised by the presence of ice, formed from the freezing of oceanic water. Such layer of sea ice is a key component of the Earth Climate System [1, 2], for it represents a sort of 'boundary condition' for heat, momentum and mass exchange between ocean and atmosphere at high latitudes [3–6] and plays a crucial role in the salinity balance in the ocean [7, 8], thus affecting also the thermohaline circulation [9]. Moreover, sea ice turns out to be a sensitive indicator of climate change: during the last few decades its average thickness and extent decreased significantly [10–12]. This decrease is two-way coupled with global warming, which shows up particularly striking in the Arctic, via the so called ice-albedo feedback. Sea ice, in fact, has a large albedo as compared to open oceanic waters, i.e. it reflects a high fraction of the incident solar radiation, while water absorbs it, thus favouring warming. The warmer the Earth surface the more ice melts, the lower gets the global albedo. The variability of sea ice emerges as the result of many processes acting on different time scales: the energy budget involving incoming and outgoing radiation [13–15], the melting phase transition [16, 17], the transport of water through ice porous structure [18–21], the rheology of internal stresses [22–25], the transport forced by couplings with ocean and atmosphere [26–31]. All these make sea ice an extremely complex system and its theoretical modelling a challenge [1, 2, 32, 33].

An important role in the ice-albedo feedback is played by the presence, on the ice surface, of melt ponds [34, 35]: during summer both the snow cover and the upper surface of sea ice melt and, as a consequence, meltwater may accumulate in depressions of the ice topography (thus forming ponds). The albedo of a melt pond ranges between $\sim$0.1 and $\sim$0.5 [36], while that of ice between $\sim$0.4 and $\sim$0.8 [34]. The average albedo for ponded ice is, then, lower than for the unponded one [37]. The evolution of melt ponds and of their distribution over the sea ice surface is, therefore, a key ingredient to be accounted for in realistic models of sea ice. It has been indeed suggested that a missing or improper inclusion of melt ponds could be the cause of overestimation, by certain general circulation models (GCMs), of the September sea ice minimum [38, 39]. For climatological temporal scales, it is important to get an accurate enough knowledge of the pond depth and surface area distributions, since these ones impact on the radiation budget; the rate of heat transfer through the ice pack, moreover, depends on the dynamics of meltwater, which, despite the average shallowness of ponds, can be turbulent [40].

The complexity of the melt-pond-covered sea ice system resides exactly in this intrinsic multiscale nature. Borrowing terms from Condensed Matter Physics, one can say that a modellistic approach may be tackled, at least, at three level of description: a *microscopic* level, where the focus is on the "atoms" of the system, the single pond and the fluid dynamics inside it, as done in, e.g., [41, 42]; a *mesoscopic* level, where the evolution of many ponds is considered, coupled with the evolution of a resolved sea ice topography [43–46]; and, finally, a *macroscopic* level, on scales of climatological interest, where sea ice dynamics is described in terms of

an ice thickness distribution (ITD) [47–49], and melt ponds need to be parametrized [38, 50, 51]. The aim of this contribution is twofold. We will propose a *mesoscopic* model (in the sense explained above) and employ it to assess the sensitivity of the melt-ponds-covered sea ice system to different modelling of certain dynamical processes occurring at the single pond *microscopic* level.

The paper is organized as follows: in Sect. 2 we introduce the proposed mathematical model and its numerical implementation; in Sect. 3 the main results are illustrated and discussed, while concluding remarks and research outlooks are left to Sect. 4.

2 The Mathematical Model

The physical processes that occur within the ice pack and lead to variation of the sea ice thickness, can be grouped essentially into two categories: thermodynamic and mechanical. Thermodynamic processes are those related to the radiative budget; the fraction of incoming radiation that is absorbed is spent to increase the surface temperature and to melt ice. Mechanical deformations of sea ice are induced by ocean and wind stresses. These can drive sea ice transport, as well as elasto-plastic deformations in the pack, giving rise to events such as ridging and rafting [1]. Since we are interested in simulating processes involving ice melting and meltwater dynamics, we will neglect sea ice transport and mechanical terms (despite they can act on time scales comparable to melting in summer). As ice melts, meltwater is formed and transported, by sliding over the ice topography and seepage through its porous structure. It will eventually concentrate in *local minima* of the ice topography, forming melt ponds.

2.1 The Sea-Ice-Thickness/Melt-Pond-Depth System

We consider, therefore, the evolution of the ice (of density ρ_i) thickness field $h(\mathbf{x}, t) \geq 0$ and the meltwater (of density ρ_w) pond depth field $w(\mathbf{x}, t) \geq 0$ (with $\mathbf{x} \in \Omega \subset R^2$), whose dynamical equations read:

$$\begin{aligned} \partial_t h &= -f \\ \partial_t w &= -\nabla \cdot (\mathbf{u} w) + \frac{\rho_i}{\rho_w} f - s, \end{aligned} \tag{1}$$

where f, $\mathbf{u}w$ and s represent, respectively, the melting rate, the meltwater flux (per unit cross-sectional area) and the seepage rate, which are, in general, functionals of h and w.

Similar mesoscopic models based on the evolution of h and w have been proposed in the past [43, 46]. Here, the original contributions to the modelling are

in the parametrization of fluid-dynamics processes, in particular the water transport term and, more importantly, the vertical and lateral melt-rate term in turbulent flow conditions, which we will describe in detail in the following.

2.1.1 Melting Rate

The precise description of the energy budget at the sea ice cover, involving incoming and outgoing radiations and the thermodynamics of ice, can be quite a challenging task [13–15]. Being the focus of our study, though, a particular aspect of the melting process, namely the reduced albedo by meltwater covering the sea ice surface, we adopt a simple modelling [43], that proves, on the other hand, to be suitable to straightforward generalizations for the problems of interest here. We write the total melting rate f appearing in (1) as the sum of two terms

$$f = (1 - \chi)\phi_1(w) + \chi\phi_2(w, \nabla w, \nabla h); \tag{2}$$

here, the first term, ϕ_1, is *local*, in fact it depends only on the pond depth $w(\mathbf{x}, t)$, whereas the second term, ϕ_2, includes also *lateral melting* mechanisms and may, thus, in principle depend also on gradients of the pond depth and ice thickness fields. The binary variable $\chi \in \{0, 1\}$ has been introduced to switch on ($\chi = 1$) or off ($\chi = 0$) such lateral melting contribution. Let us first discuss the local term ϕ_1. We assume a constant melting rate $\phi_1 = m_i$, of dimensions [length/time], for *bare* (unponded) ice (i.e. if $w(\mathbf{x}, t) = 0$), which is magnified by a w-dependent factor $\mathscr{A}(w)$, if ice is covered by a pond ($w(\mathbf{x}, t) > 0$); altogether, the expression for ϕ_1 reads:

$$\phi_1(w) = \mathscr{A}(w)m_i. \tag{3}$$

Following Lüthje et al. [43], one can take $\mathscr{A}(w)$ to be:

$$\mathscr{A}(w) = \begin{cases} 1 + \frac{m_p}{m_i}\frac{w}{w_{\max}} & \text{if } w \in [0, w_{\max}] \\ 1 + \frac{m_p}{m_i} & \text{otherwise} \end{cases} \tag{4}$$

where m_p is a (constant) limit melting rate for ponded ice, when the overlying pond depth exceeds the value $w_{\max}$ (which is usually estimated to be pretty small, $w_{\max} \approx 0.1$ m, because turbulent convection is already relevant at such depth, as discussed later on). The meaning and origin of such magnifying factor deserves some comments. In very shallow ponds, $w < w_{max}$, as a consequence of the absorption of solar radiation by water, the warming up is proportional to its volume and so the heat flux through the liquid layer is proportional to w. The situation changes for slightly deeper ponds, $w > w_{max}$, due to the appearance of natural convection. Indeed in summertime the temperature of air in contact with ponds

($\approx$2 °C) is higher than the basal one, in contact with melting ice (at 0 °C). In this range water density shows the well known anomaly, according to which it decreases with temperature, $\rho_w(T = 2\,°\text{C}) > \rho_w(T = 0\,°\text{C})$, therefore, the pond is prone to convection. The latter sets on when the system becomes dynamically unstable; this will occur when the pond depth, which grows in time because of melting (thus making the system intrinsically non-stationary), will reach a value such that the time-dependent Rayleigh number $Ra(t)$ is large enough. The Rayleigh number quantifies the relative magnitude of buoyancy and dissipative terms; grouping together water density ρ_w, thermal expansion coefficient β, dynamic viscosity η, thermal conductivity κ and specific heat capacity at constant pressure c_p with gravity yields:

$$Ra(t) = \frac{c_p \rho_w^2 \beta g (\Delta T) w(t)^3}{\kappa \eta}, \tag{5}$$

Although it may seem surprising, the ponds being in general shallow, if we plug typical values in (5) we get, even for $w \approx 0.1$ m and $\Delta T \approx 0.2\,°\text{C}$, $Ra \approx 10^6$ [40], a value at which convection is already moderately turbulent [52]. Within ponds of depth $w \gtrsim 0.1$ m, filled of fresh water, heat is not transferred by conduction, but by turbulent convection, whence the larger basal melting rate (3)–(4). For the sake of simplicity we neglect here salt concentration. Such an assumption must be taken with due care, though, since salinity hinders convection, by density stratification, and can even inhibit it (as shown in [53]).

The dependence of the total heat flux in turbulent conditions Φ_{turb} (in W/m^{-2} units) on the depth, though, is a complex problem. Expressed in non-dimensional variables, it amounts to assessing the Nusselt Nu *vs* Rayleigh numbers scaling $Nu \sim Ra^c$ [52, 54], where the Nusselt number is defined as:

$$Nu(t) = \frac{\Phi_{\text{turb}}(t)}{\kappa \frac{(\Delta T)}{w(t)}}. \tag{6}$$

The expression (4) arises from the assumption of the so called Malkus scaling $Nu \sim Ra^{1/3}$ [55]. Note that this scaling corresponds to the conjecture that the turbulent heat flux is independent of the thickness of the liquid layer, and as a consequence that the melt rate is fixed at a constant value m_p as stated by (4) in the model by Lüthje et al. [43] or by Taylor and Feltham [40]. However, theories, experiments and numerical simulations tend to agree that, in the range of Ra of relevance for melt pond convection, the scaling exponent should be $c < 1/3$ (see, e.g., [54] and references therein); in particular, widely observed is $Nu \sim Ra^c$, with $c \approx 2/7$. A similar scaling was observed, in numerical simulations, also for turbulent thermal convection with phase transition, where a boundary evolves, driven by melting [42], a setup which more closely resembles what occurs inside a melt pond. So, we propose to generalize Eqs. (3)–(4) for the local magnitude of

melting to a generic $Nu \sim Ra^c$ relation and we obtain:

$$\phi_1(w) = m_i + m_p(w,c)\left(\frac{w}{w_{\max}}\right)^{\alpha}, \quad \text{with } \alpha = \begin{cases} 1 & \text{if } w \in [0, w_{\max}] \\ 3c-1 & \text{if } w > w_{\max}, \end{cases} \tag{7}$$

so that for ponds deeper than w_{max} Lüthje et al.'s case [43] is recovered for $\alpha = 0$, while scaling exponent equal to $2/7$ yields for $\alpha = -1/7$. Notice that we have allowed also the constant m_p to be depth dependent in our model, $m_p \to m_p(w)$. This is done in order to include another aspect of realistic convection in Arctic ponds: the effect of a surface wind shear. At high latitudes, in fact, strong wind shear from the atmospheric boundary layer is present that can affect significantly sea ice dynamics (e.g. in the formation of sea-ice bridges [56]). Artic winds act on pond surfaces and are able, in principle, to strongly modify the convection patterns [41]. In such situations, turbulent heat flux is initially depleted, due to thermal plumes distortion by the shear [57, 58], and then it increases again, when turbulent forced convection becomes the dominant mechanism. On the line of the same arguments exposed in [58], based on Prandtl's mixing length theory [59], an expression for the coefficient $m_p(w)$ of the following form

$$m_p(w,c) \sim m_p^{(0)}(w,c)\left(\frac{a_1}{1 + c_1(\tau_s)w^{\gamma_1}} + a_2 c_2(\tau_s) w^{\gamma_2}\right), \tag{8}$$

can be expected, where a_1 and a_2 are some phenomenological parameters and c_1 and c_2 are functions of the wind shear magnitude τ_s (and of physical properties of meltwater). In all numerical results reported here, however, we have set $\tau_s = 0$, that is we have kept $m_p(w) \equiv m_p^{(0)}(w,c)$ (exploring wind shear effects will be object of a forthcoming study). The dependence of $m_p^{(0)}(w,c)$ on w and c stems from the fact that: (i) below w_{max} the heating is mainly radiative and (ii) changing the exponent of the scaling relation between dimensionless quantities, $Nu \sim Ra^c$, affects also the prefactor of the turbulent heat flux, i.e. $\Phi_{\text{turb}} = A(c)w^{3c-1}$. The expression for $m_p^{(0)}(w,c)$ therefore reads:

$$m_p^{(0)}(w,c) = \begin{cases} m_{p,r}^{(0)} & \text{if } w \in [0, w_{\max}] \\ b_c(Pr)\left(\frac{c_p \rho_w^2 \beta g}{\eta}\right)^c \kappa^{1-c}(\Delta T)^{1+c} & \text{if } w > w_{\max}, \end{cases} \tag{9}$$

where the coefficient $b_c(Pr)$ depends on the Prandtl number, $Pr = c_p\eta/\kappa$. As previously commented, Eq. (7) is purely local and "vertical", in the sense that, if we think in discrete time, in a step Δt, it would increase the pond depth by $\phi_1(w(\mathbf{x},t))\Delta t$, $w(\mathbf{x},t) \to w(\mathbf{x},t) + \frac{\rho_i}{\rho_w}\phi_1(w(\mathbf{x},t),t)\Delta t$, and decrease the ice thickness by $h(\mathbf{x},t) \to h(\mathbf{x},t) - \phi_1(w(\mathbf{x},t))\Delta t$, without affecting or being affected

by the neighbourhood. We may expect, though, that, due to convection induced mixing, meltwater will be at a higher temperature than the surrounding ice and it may, therefore, favour melting also horizontally. This can be especially relevant close to the edge of pond surfaces, where it should give rise to a widening of ponds. To account for this kind of mechanism, we have introduced in the expression for the total melting rate, Eq. (2), the term $\phi_2(w, \nabla w, \nabla h)$, which contains the lateral melting (its explicit lattice expression will be given in Sect. 2.2). An attempt to estimate lateral fluxes in pond convection was proposed by Skyllingstad and Paulson [41], though with prescribed and fixed (with no evolving boundaries) forms of ponds. Finally, it is important to underline that by "lateral melting" we refer here to horizontal melting within the pond, and not edge melting of the ice pack, as when interactions with the ocean are considered [60].

2.1.2 Seepage Rate

Sea ice has a complex porous structure that evolve in time as the pack melts [19, 61]; a thorough description of water percolation through it is a formidable task that goes beyond the scope of the present work. We just model water transport through sea ice using Darcy's law; in addition, we distinguish between vertical and horizontal transport [43, 46]. Vertical transport is accounted for in Eqs. (1) by the seepage term s; the horizontal contribution, also dubbed lateral drainage, will be discussed in the next subsection. In order to derive an expression for the seepage rate, we recall that, according to Darcy's law, the discharge through volume of homogeneous porous material of permeability k, cross-sectional area a and length ℓ, under an applied pressure difference $(p_{\text{in}} - p_{\text{out}})$, is given by

$$q = k\frac{a(p_{\text{in}} - p_{\text{out}})}{\eta\ell}; \tag{10}$$

for a portion of ponded ice of elementary area δa and thickness h, such pressure head is due to the hydrostatic pressure of the column of water in the pond overlying ice on δa, whose height is w, is $(p_{\text{in}} - p_{\text{out}}) = \rho_w g \delta a w$. The discharge q equals the time variation of the overlying volume of water, $\dot{\mathcal{V}} = \delta a \dot{w}$, providing

$$\dot{w} = -k\frac{\rho_w g w}{\eta h}, \tag{11}$$

out of which we can read the expression for the seepage rate s that is [46]

$$s = k\frac{\rho_w g}{\eta}\frac{w}{h}. \tag{12}$$

2.1.3 Meltwater Flux

The seepage rate just introduced, Eq. (12), entails a dependence of the equation for $w(\mathbf{x}, t)$ on $h(\mathbf{x}, t)$ (that would be otherwise be decoupled from it, as far as only melting is concerned). A further coupling is induced by the transport term and the associated meltwater flux $\mathbf{u}$. Such term is also the only non-local one in the evolution (for it involves derivatives of h and w), thus introducing a dependence of the dynamics on the ice topography. It represents, in other words, the driving for meltwater to accumulate to form ponds. The transport of meltwater is realised essentially with two mechanisms: *sliding* of water over slopes of the ice surface and *lateral drainage* through the porous structure of ice. Correspondingly, the flux consists of the sum of two terms

$$\mathbf{u} = \mathbf{u}_{\text{sliding}} + \mathbf{u}_{\text{drainage}}; \tag{13}$$

as discussed in the previous subsection, $\mathbf{u}_{\text{drainage}}$ stems from the horizontal component of Darcy's law and, hence, is given by [43]

$$\mathbf{u}_{\text{drainage}} = -\Pi \frac{\rho_w g}{\eta} \nabla(h + w), \tag{14}$$

where Π is the horizontal permeability of ice.

In order to model the sliding term, we resort to the theory of shallow water equations (SWE) [62], considering that the width of a layer of water sliding over the ice topography is relatively thin. If we assume, furthermore, that the Reynolds number is small (we expect so, and a consequent creeping flow, for a thin layer of water sliding over the ice topography, the thickening of such layer being inhibited by seepage), the SWE for the depth-averaged two-dimensional velocity field reduce to the following balance equation between stresses at the bottom (due to friction with ice) and top (induced by wind forcing) of the fluid layer and gravity [63, 64] (assuming a no-slip boundary condition between water and ice and neglecting capillary effects)

$$\frac{3\eta}{w} \mathbf{u}_{\text{sliding}} + \tau_s + g w \nabla(h + w) \approx 0, \tag{15}$$

which yields for $\mathbf{u}_{\text{sliding}}$:

$$\mathbf{u}_{\text{sliding}} = -\frac{g w^2}{3\eta} \nabla(h + w) + \frac{\tau_s w}{3\eta} \hat{\tau}_s, \tag{16}$$

where $\hat{\tau}_s$ is the direction of the wind shear vector at the free water surface and τ_s is its magnitude, as in Eq. (8). Let us stress that, in this way, we have introduced, through Eqs. (8) and (16) a first minimal coupling of the model for the sea-ice-melt-ponds system with the atmospheric dynamics.

2.2 Numerical Implementation

The system of equations (1) is solved by means of a finite differences scheme; upon discretization on a square $M \times M$ lattice, with $M = 1024$, of equally Δ-spaced nodes, the system is converted in a set of coupled ordinary differential equations for the variables $h_{ij}(t) \equiv h(x_i, y_j, t)$ (with $x_i = i\Delta$, $y_j = j\Delta$ and $i, j = 1, 2, \ldots, M$) and $w_{ij}(t) \equiv w(x_i, y_j, t)$, that are, then, integrated numerically using a standard explicit Runge-Kutta fourth order time marching scheme with time step $\Delta t = 60\,\mathrm{s}$, that allows to resolve the fastest time scales of the meltwater transport terms. Spatial derivatives are approximated by the corresponding second order accuracy central differences. The lattice spacing Δ is taken to be $\Delta = 1\,\mathrm{m}$, so the physical size of the simulated system is $L^2 \approx 1\,\mathrm{km}^2$, where $L = M\Delta$; this choice is dictated by the condition that Δ is $\Delta \gtrsim \sigma_h$ (σ_h being the standard deviation of the initial ice thickness distribution), such that no significant variations of of h occur within one lattice spacing, i.e. the spatial derivative is at most $h'(x) \sim 1$, assuming that the average finite height variation over a Δ is $\Delta h \propto \sigma_h$. Periodic boundary conditions apply, so we neglect edge effects, such as water run-off and direct coupling with the ocean (e.g. lateral melting of floe, ocean stresses), i.e. it is as if we were simulating a virtually infinite sea ice floe.

The melting term ϕ_2, appearing in Eq. (2), takes the following expression on the lattice

$$\phi_{2_{i,j}} = \phi^{(V)}_{2_{i,j}} + \sum_{i'=\pm 1} \phi^{(L,x)}_{2_{i+i',j}} \Theta(w_{i+i',j} - w_{i,j}) + \sum_{j'=\pm 1} \phi^{(L,y)}_{2_{i,j+j'}} \Theta(w_{i,j+j'} - w_{i,j}), \tag{17}$$

which contains a combination of *vertical*, $\phi^{(V)}_{2_{i,j}}$, and *lateral*, $\phi^{(L,(x,y))}_{2i,j}$, components of the melting; the latter are given by:

$$\phi^{(V)}_{2_{i,j}} = \phi_{1_{i,j}} \frac{1}{\sqrt{1 + (\hat{\partial}_x w_{i,j})^2 + (\hat{\partial}_y w_{i,j})^2}} \tag{18}$$

and

$$\phi^{(L,(x,y))}_{2,i,j} = \phi_{1_{i,j}} \frac{|\hat{\partial}_{(x,y)} w_{i,j}|}{\sqrt{1 + (\hat{\partial}_x w_{i,j})^2 + (\hat{\partial}_y w_{i,j})^2}}, \tag{19}$$

where $\hat{\partial}_{(x,y)}$ stands for the finite difference derivative. We assume that the magnitude of the turbulent heat flux is homogeneously distributed over the pond walls (that is at the ice/water interface) and its direction is parallel to the normal $\hat{n}$ to the interface. Therefore, the vertical and lateral contributions to the melting rate are weighted with

the absolute values of the components of $\hat{n}$,

$$\frac{1}{\sqrt{1+(\hat{\partial}_x w_{i,j})^2+(\hat{\partial}_y w_{i,j})^2}}\left(|\partial_x w|, |\partial_y w|, 1\right),$$

whence Eqs. (18) and (19). In other words, this means that, for instance, at the bottom of the pond mostly the vertical term will act, while when the topography is steep, as, e.g., next to the pond edge, ice ablation will be dominated by lateral melting. The presence of the Heaviside's functions, Θ, in (17) is to guarantee that the, non-local, lateral contribution to melting on a given site comes only from those neighbours that have a larger amount of overlying water (larger w). This is motivated by the idea that, if at a given elevation H a certain site is in the 'ice state', it will get a lateral melting contribution from a neighbouring site which, at the same elevation, is in a 'water state', since melting is driven by water convection in contact with ice enclosing the pond.

3 Results

The initial values of the sea ice topography $h^0_{ij} \equiv h(x_i, y_j, 0)$ are random Gaussian numbers with given mean and variance. The initial topography is spatially correlated over a characteristic length $\delta \approx 8$ m. Two types of ice are used as initial conditions, namely first-year ice (FYI) and multi-year ice (MYI). FYI is newly formed in the winter preceding the melt season and is typically flatter, whereas MYI, that has overcome one or more melt seasons, presents a more rugged surface profile, i.e. it is characterized by larger variance and mean as compared to FYI. Consequently, wide and ramified but shallow melt ponds are more probably formed on FYI, while melt ponds on MYI will be tendentially deeper, of limited areal extension and more regularly shaped [50]. The initial condition is therefore expected to play an important role on the meltwater dynamics. The statistical parameters (mean $\langle h \rangle$ and variance σ_h of the thickness distribution) employed are $\langle h \rangle = 0.92$ m, $\sigma_h = 0.18$ m, for FYI, and $\langle h \rangle = 3.67$ m, $\sigma_h = 1.5$ m, for MYI [43, 65]. Other numerical values for the model parameters, which are kept fixed in all simulations, are summarized in Table 1. Evidently, we are faced to a wide, multi-dimensional, parameter space; many of these parameters (such as permeabilities and melting rates) are known only with limited accuracy and the system can be quite sensitive to their values. A full sensitivity study in such sense is somehow beyond the scope of the present work; moreover some studies of this kind (on similar models) are available (see, e.g. [43, 46]). We limit here ourselves, therefore, to test the novelties of the present model, namely the melting rate exponent associated to turbulent thermal convection and its contribution along the lateral (horizontal) directions.

Table 1 Values of model parameters which are kept fixed in all simulations: water density ρ_w, ice density ρ_i, water dynamic viscosity η, acceleration of gravity g, horizontal permeability of ice Π, *bare* ice melting rate m_i, melting rate enhancement factor $m_p^{(0)}$ and critical pond depth for melting rate enhancement $w_{\max}$

Parameter	ρ_w	ρ_i	η	g	Π	m_i	$m_p^{(0)}$	$w_{\max}$
Units	$\mathrm{kg/m^3}$	$\mathrm{kg/m^3}$	$\mathrm{kg/(m\,s^{-1})}$	$\mathrm{m/s^2}$	$\mathrm{m^2}$	cm/day	cm/day	m
Value	1000	950	1.79×10^{-3}	9.81	3×10^{-9}	1.2	2	0.1

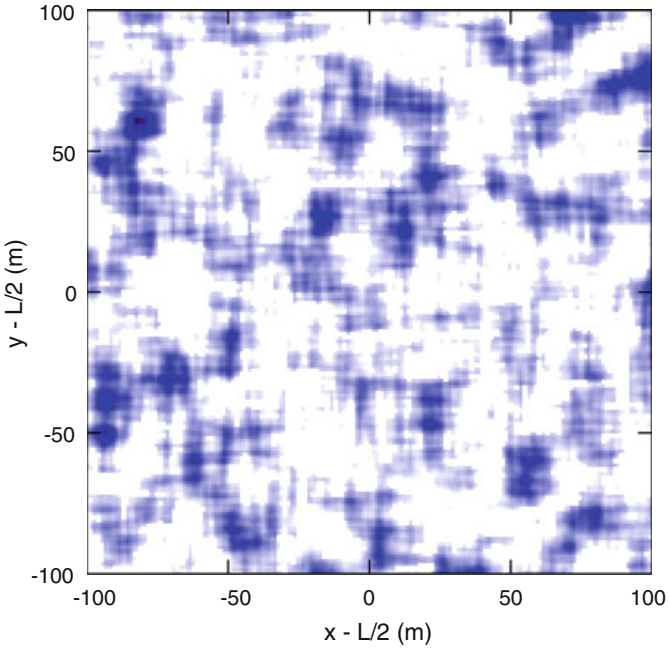

Fig. 1 Configuration of the depth field $w(\mathbf{x}, t)$ showing the melt ponds distribution over the sea ice surface, for FYI after 20 simulated days (a $200 \times 200\,\mathrm{m}^2$ region at the centre of the simulated domain is taken). White color corresponds to bare ice and blue color indicates the presence of a pond, the darker the blue the deeper the pond (deepest ponds have $w \approx 2\,\mathrm{m}$) (Color figure online)

Snow cover is absent and no melt water is assumed at the initial time (i.e. $w(\mathbf{x}, t_0) = 0 \quad \forall \mathbf{x}$). As said before, we aim to simulate the summer time evolution of sea ice, so our t_0 is to be considered June 1st and, in view of this, refreezing of meltwater is not accounted for. We ran each simulation for ≈30 days. A visualization of the distribution of ponds corresponding to day 20 from the beginning of the simulation is shown in Fig. 1. In order to extract statistical information on the melt pond coverage of the sea ice, we first need to identify individual ponds. To do this, for each time t we define a pond as any connected subset of points on the lattice such that $w(\mathbf{x}, t) > 0$; the full pond configuration is determined by a cluster analysis (for which we employ the so called Hoshen-Kopelman algorithm [66]) over the whole system. The area of the i-th pond is then $A_i = n_i \Delta_x \Delta_y$, n_i being the number of points in the i-th cluster.

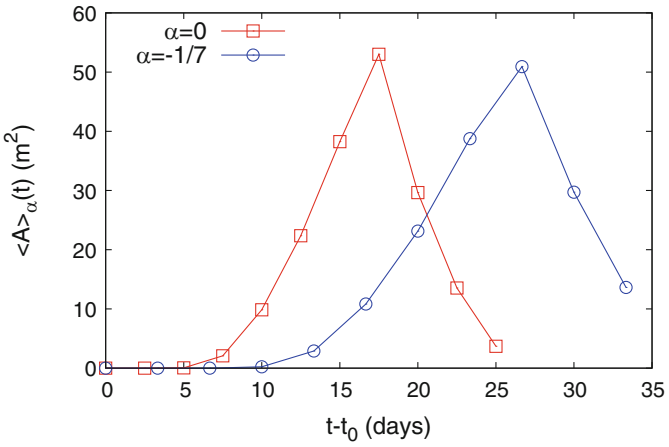

Fig. 2 Mean pond area vs time for the 1/3 (red squares) and 2/7 (blue circles) laws (Color figure online)

3.1 Melt Pond Areas Evolution: Role of the Turbulent Heat Flux Scaling Inside the Pond

In Fig. 2 we plot the time evolution of the mean pond area

$$\langle A\rangle_\alpha(t) = \frac{1}{N(t)}\sum_{i=1}^{N(t)} A_i(t) \tag{20}$$

(where $N(t)$ is the total of ponds detected at time t) for a FYI and assuming Malkus and 2/7 scaling for the turbulent heat flux, respectively, that is, with reference to Eq. (7), with $\alpha = 0$ (red squares, equivalent to the study in [43]) and $\alpha = -1/7$ (blue circles). The mean pond area grows and reaches a maximum faster when $\alpha = 0$: after 13 days, e.g., the 2/7-model gives a prediction for $\langle A\rangle_\alpha$ approximately seven times smaller than it is for the constant flux case; this suggests how an apparently minor assumption at the level of fluid dynamic processes within the single pond may lead to bad estimates on climatologically relevant indicators, such as the September sea ice extension. For the same two runs, with $\alpha = 0, -1/7$, we measured the probability distribution functions (PDFs) of pond areas, $P_\alpha(A, t)$, after 13 days; one can see from Fig. 3 that the two PDFs differ, although both seem to show a power law behaviour. Nevertheless, if we consider PDFs with *equal mean*, instead of *equal time* PDFs, interestingly, the two sets of points (for $\alpha = 0$ and $\alpha = -1/7$) collapse onto each other, as shown in Fig. 4. There we plot $P_{\alpha=0}(A, t_1)$ and $P_{\alpha=-1/7}(A, t_2)$, where t_1 and t_2 are such that $\langle A\rangle_{\alpha=0}(t_1) = \langle A\rangle_{\alpha=-1/7}(t_2)$; with reference to Fig. 2, this occurs, for instance, if we pick $t_1 - t_0 = 13$ days and $t_2 - t_0 = 20$ days, i.e. on June 14th for $\alpha = 0$ and June 21st for $\alpha = -1/7$. The two PDFs nicely follow the scaling $P_\alpha(A) \sim A^{-1.5}$ for relatively small areas ($A < 20\,\mathrm{m}^2$), with